# AUTONOMOUS FORMATION KEEPING AND RECONFIGURATION FOR REMOTE SENSING SPACECRAFT

**S. D'Amico[(1)], S. De Florio[(1)], R. Larsson[(2)], M. Nylund[(2)]**

*[(1)] German Aerospace Center (DLR), Münchner Str. 20, 82234 Wessling, Germany*
*[(2)] Swedish Space Corporation (SSC), Strandväg 86, P.O.Box 4207, Solna, Stockholm, Sweden*

## ABSTRACT

This paper is devoted to the realistic demonstration of a complete Guidance, Navigation and Control (GNC) system for formation flying spacecraft in Low Earth orbit (LEO). Numerous technical novelties in the areas of formation flying guidance, GPS-based relative navigation, and impulsive relative orbit control have made this possible, but the primary contribution of this research work stems from the design and implementation of a comprehensive formation flying system through the successful integration of various techniques. This research has led to the full development, testing and validation of the GNC flight code to be embedded in the on-board computer of the *Main* spacecraft of the Swedish PRISMA technology demonstration. Furthermore key guidance and control algorithms presented here are going to be demonstrated for the first time on-board the German TanDEM-X formation flying mission. Overall this paper focuses on realistic application cases closely related to upcoming formation flying missions. The intention is to realize a practical and reliable way to a technology which is discussed and studied since decades but is still confined in research laboratories. Hardware-in-the-loop real-time simulations including flight computers show that simple techniques, which exploit the natural orbit motion to full extent, can meet the demanding requirements of the long-term close formation flying.

## INTRODUCTION

Although using the Hill frame coordinates [1] is a common method to describe the satellites relative motion, they have the distinct disadvantage that for a general orbit the differential equations of motions must be solved to obtain the precise instantaneous geometry of the formation. Because of this fact, here a description in terms of relative orbital elements has been preferred to the canonical Cartesian parameterization. In contrast to the fast varying position and velocity variables, the use of orbital element differences simplifies the formation-flying description and the satellite relative position computation. Various sets of relative orbital elements have been proposed in the past decades in the frame of formation-flying dynamics and control [2], but actually the most intuitive, straightforward representation in terms of relative eccentricity and inclination vectors has never been investigated for formation-flying design in LEO. This research generalizes the method of eccentricity/inclination vector separation, first developed for the safe collocation of geostationary satellites [3], and extends its application to proximity operations of formation-flying spacecraft. The spontaneous geometrical representation offers a direct correlation between the relevant characteristics of the bounded relative motion in near circular orbit and the magnitude/phase of the relative eccentricity/inclination vectors. This aspect extremely simplifies the design of safe, passively stable formation-flying configurations. In particular minimum collision risk conditions can be guaranteed by imposing the (anti-)parallelism of the eccentricity and inclination vectors of the respective satellites, while $J_2$-stable relative orbits are obtained by setting a specific nominal phase for the configuration. The new approach is shown to be suitable either for the realization of SAR interferometers with baselines below 1 km [4] or the application in longitude swap operations with along-track separations above 200

km [5]. This paper addresses the first case where an active relative orbit control strategy is necessary, in order to compensate for the main disturbance forces represented by Earth's oblateness perturbations and differential aerodynamic drag. The required velocity budget for formation-keeping can be expressed in terms of relative orbital elements and is directly proportional to the relative eccentricity and inclination offsets. Furthermore the proposed analytical solution is adopted to reconfigure the formation in a safe and fuel-efficient way.
The results obtained so far by various authors demonstrate that carrier-phase differential GPS is an invaluable source of relative navigation in LEO [6]. The use of space-borne GPS receivers and true GPS signals in their hardware simulations mark a major progress on the way to acquire flight experiments. Nevertheless some limitations characterize the previous studies and, as a consequence, are addressed in this research. First of all the navigation concepts available in literature do not incorporate maneuvers, which is crucial for use in formation keeping and reconfiguration. Secondly the handling of the spacecraft attitude and the robustness of the filter to non-ideal non-zenith orientations of the GPS antennas are neglected. Last but not least contingency scenarios or delicate formation-flying operations phases like the launch and early operations phase or the safe separation of the spacecraft from a common combined configuration are typically not addressed. The weakness of previously designed filters makes the strength of this development. In contrast to earlier approaches that separate the GPS-based navigation into the independent reconstruction of absolute and relative states, a single reduced-dynamic Kalman filter for the absolute states of both spacecraft has been adopted in this work. Two different types of measurements are processed by the filter: undifferenced GRAPHIC [7] measurements of the individual spacecraft as well as single-difference carrier-phase measurements. Both data types are practically ionosphere-free for short separations [8] and are subject to ambiguities related to the nature of carrier phase measurements. Channel specific ambiguities must therefore be estimated as part of the navigation filter. The inherent robustness of the symmetric filter design originates from the fact that common GPS satellites visibility is not a prerequisite to reconstruct the relative state. Even in the case of spacecraft with completely different attitude, the relative state can be determined by simply differencing absolute estimates exclusively based on GRAPHIC data types. The unified filter design simplifies the initialization and the maneuver handling procedures, and, consequently, improves the flexibility of the navigation system and its reliability during formation flying experiments.
Finally this paper addresses the testing and validation of the GNC flight software once integrated into the PRISMA [9] spacecraft on-board computer. Thanks to a novel model-based software design, the GNC software is implemented and executed on different platforms in a fully consistent manner. This allows a seamless transition between off-line, real-time and hardware-in-the-loop environments during the validation phase. Results from a long-term representative real-time hardware-in-the-loop simulation conducted in the Satellite Laboratory (SATLAB) at the Swedish Space Corporation (SSC) are presented. Overall the test and validation process shows the compliance of the GNC system to the challenging requirements of PRISMA and paves the way for the upcoming launch and mission operations.

# 1 FORMATION FLYING GUIDANCE AND CONTROL

## 1.1 Relative motion model

The formation under investigation is composed of a chief and a deputy satellite. The chief satellite is taken as the reference of the formation and is the spacecraft about which the deputy satellite is orbiting. Here the adopted denomination is completely arbitrary and does not imply any privileged or specific responsibility to the chief satellite with respect to the deputy. The relative motion of the deputy with respect to the chief satellite can be parameterized through an appropriate set of relative orbital elements

$$\delta \boldsymbol{\alpha} = \begin{pmatrix} \delta a \\ \delta \lambda \\ \delta e_x \\ \delta e_y \\ \delta i_x \\ \delta i_y \end{pmatrix} = \begin{pmatrix} (a_d - a)/a \\ (u_d - u) + (\Omega_d - \Omega)\cos i \\ e_{x_d} - e_x \\ e_{y_d} - e_y \\ i_d - i \\ (\Omega_d - \Omega)\sin i \end{pmatrix}, \tag{1}$$

which are obtained by a non-linear combination of the absolute orbital elements. Here the subscript *d* is introduced to denote quantities related to the deputy satellite and to distinguish them from the orbital elements of the chief spacecraft. The semi-major axis difference $\delta a$ has been normalized through the chief semi-major axis to have dimensionless quantities. $\delta\lambda$ denotes the relative mean longitude between the spacecraft, and is defined based on the differences in mean argument of latitude $u = \omega + M$ and right ascension of the ascending node $\Omega$. Apart from $\delta a$ and $\delta\lambda$, the relative orbit representation defined by Eq. (1) is based on the relative eccentricity and inclination vectors for which the following polar notations can be applied

$$\delta \boldsymbol{e} = \delta e \begin{pmatrix} \cos\varphi \\ \sin\varphi \end{pmatrix} \quad \text{and} \quad \delta \boldsymbol{i} = \delta i \begin{pmatrix} \cos\vartheta \\ \sin\vartheta \end{pmatrix}. \tag{2}$$

The amplitudes (or lengths) of the relative e/i-vectors are denoted by $\delta e$ and $\delta i$ respectively and should not be confused with the arithmetic differences of eccentricity and inclination for which the $\Delta(\bullet)$ operator is used. The phases of the relative e/i-vectors are termed relative perigee $\varphi$ and relative ascending node $\vartheta$ because they characterize the geometry of the relative orbit as seen by the chief spacecraft.

A common way to parameterize the absolute orbit motion of a spacecraft about a central body is to adopt the Cartesian coordinates state vector $\boldsymbol{x} = (\boldsymbol{r}\ \boldsymbol{v})^T$, being $\boldsymbol{r} = (\boldsymbol{r}_x\ \boldsymbol{r}_y\ \boldsymbol{r}_z)^T$ the orbit position vector and $\boldsymbol{v} = (\boldsymbol{v}_x\ \boldsymbol{v}_y\ \boldsymbol{v}_z)^T$ the orbit velocity vector in the Earth Centered Inertial (ECI) frame. Similar to the orbital elements representation, the relative motion of two co-orbiting satellites can be described by a set of relative Cartesian coordinates obtained by the combination of the individual state vectors. To this end we introduce the Hill orbital frame as a natural basis of measurements and scientific observations [1]. Its origin is at the chief position and its orientation is given by the vector triad $(\boldsymbol{o}_r\ \boldsymbol{o}_t\ \boldsymbol{o}_n)^T$. The unit vector $\boldsymbol{o}_r$ is aligned with the radial direction (positive outwards), while $\boldsymbol{o}_n$ is parallel to the chief angular momentum vector (positive in the orbit normal direction). The vector $\boldsymbol{o}_t$ completes the right-handed coordinate system (positive in chief velocity direction). The relative motion of the deputy with respect to the chief spacecraft can be expressed through Hill coordinates as

$$\delta \boldsymbol{x} = \begin{pmatrix} \delta r_r \\ \delta r_t \\ \delta r_n \\ \delta v_r \\ \delta v_t \\ \delta v_n \end{pmatrix} = \begin{pmatrix} \Delta\boldsymbol{r} \cdot \boldsymbol{o}_r \\ \Delta\boldsymbol{r} \cdot \boldsymbol{o}_t \\ \Delta\boldsymbol{r} \cdot \boldsymbol{o}_n \\ \Delta\boldsymbol{v} \cdot \boldsymbol{o}_r + \Delta\boldsymbol{r} \cdot \dot{\boldsymbol{o}}_r \\ \Delta\boldsymbol{v} \cdot \boldsymbol{o}_t + \Delta\boldsymbol{r} \cdot \dot{\boldsymbol{o}}_t \\ \Delta\boldsymbol{v} \cdot \boldsymbol{o}_n + \Delta\boldsymbol{r} \cdot \dot{\boldsymbol{o}}_n \end{pmatrix}. \tag{3}$$

As mentioned above, the $\Delta(\bullet)$ operator indicates arithmetic differences between absolute Cartesian parameters, while $\delta(\bullet)$ refers to a non-linear combination of the formers. Under the assumptions of a Keplerian two-body motion, a circular chief orbit, and spacecraft separations

which are small as compared to the chief orbit radius, the fundamental equations of dynamics can be linearized to obtain the familiar Clohessy-Wiltshire (C-W) equations of relative motion [10]. These equations have the following convenient homogeneous analytical solution for the relative position and velocity

$$\begin{aligned}
\delta r_r &= a_1 - a_3 \cos nt - a_4 \sin nt && = a_1 - a_{34} \cos(nt - \varphi) \\
\delta r_t &= a_2 - 1.5na_1(t - t_0) + 2a_3 \sin nt - 2a_4 \cos nt && = a_2 - 1.5na_1(t - t_0) + 2a_{34} \sin(nt - \varphi) \\
\delta r_n &= a_5 \sin nt - a_6 \cos nt && = a_{56} \sin(nt - \vartheta) \\
\delta v_r &= na_3 \sin nt - na_4 \cos nt && = na_{34} \sin(nt - \varphi) \\
\delta v_t &= -1.5na_1 + 2na_3 \cos nt + 2na_4 \sin nt && = -1.5na_1 + 2na_{34} \cos(nt - \varphi) \\
\delta v_n &= na_5 \cos nt + na_6 \sin nt && = na_{56} \cos(nt - \vartheta)
\end{aligned} \quad . \qquad (4)$$

Here $n$ represents the mean orbit motion. The amplitudes of the in-plane and out-of-plane relative motion oscillations are $a_{34} = (a_3^2 + a_4^2)^{0.5}$ and $a_{56} = (a_5^2 + a_6^2)^{0.5}$ respectively. The phases of the harmonic in-plane and out-of-plane oscillations are $\phi = \arctan(a_4/a_3)$ and $\theta = \arctan(a_6/a_5)$ respectively. It is possible to show that the relative orbital elements $\delta\boldsymbol{\alpha}$ defined by Eq. (1) match the integration constants of the C-W equations $\boldsymbol{a} = (a_j)$ with $j = 1,\ldots,6$, defined by Eq. (4) under the assumption of near-circular chief orbits and relative orbit radius small compared to the inertial orbit radius (i.e., all $\delta\boldsymbol{\alpha}$ components are small, $\delta\alpha \ll 1$ or $\delta r/r \ll 1$). It is important to make two remarks on this assumption. First of all the assumption of small relative orbit radius with respect to the inertial orbit radius does not imply that $\Delta M \ll 1$ or $\Delta\omega \ll 1$, but only that their sum $\delta u = \Delta M + \Delta\omega \ll 1$. On the contrary all other classical orbit elements differences are small. Secondly the relative orbital elements have been introduced as dimensionless or angular quantities, while all C-W integration constants have the dimension of a length for rectilinear coordinates. Here the correspondence between these vectors refers to normalized quantities with respect to the semi-major axis of the chief orbit. The demonstration of this identity is based on the direct geometrical mapping between Hill frame position coordinates and classical orbital element differences [11]. These equations are valid for arbitrary eccentricities and can be reduced to a form like Eq. (4) if orbital elements differences and eccentricity are small quantities and terms obtained by the products or powers of $\Delta(\bullet)$ and $e$ can be dropped. The original expressions can be then truncated to first-order and re-arranged to show explicitly the dependency of $\delta r_r$ and $\delta r_t$ on the relative eccentricity vector components and of $\delta r_n$ on the relative inclination vector as follows

$$\begin{aligned}
\delta r_r / a &= \delta a - \delta e \cos(u - \varphi) \\
\delta r_t / a &= \delta\lambda - 1.5\delta a(u - u_0) + 2\delta e \sin(u - \varphi) \\
\delta r_n / a &= \delta i \sin(u - \vartheta)
\end{aligned} \; . \qquad (5)$$

The general linear solution given by Eq. (5) provides the relative Cartesian position vector $\delta\boldsymbol{r}$ at any mean argument of latitude $u$ (i.e., $u$ is the independent variable) as a function of the relative orbital elements $\delta\boldsymbol{\alpha}$ at epoch $t_0$. Although $\delta a$ and $\delta\lambda$ represent classical normalized Keplerian elements differences, $\delta e$ and $\delta i$ deserve further reflections. The necessary conditions for bounded, centered relative motion of a deputy with respect to the chief spacecraft are given by $\delta a = 0$ and $\Delta u = -\Delta\Omega\cos i$. When these conditions apply, the relative orbit of the deputy with respect to chief spacecraft is an ellipse of semi-major axis $2a\delta e$ in along-track direction and semi-minor axis $a\delta e$ in radial direction (cf. Fig. 1). While $\delta e$ measures the size of the relative trajectory, the angle $\varphi$ defines the relative pericenter. Whenever the argument of latitude $u$ equals $\varphi$, the deputy is located right below the center. As

soon as $u = \varphi + \pi/2$, the deputy takes over and is just ahead of the chief satellite. In analogy with the preceding concepts, the relative inclination vector is used to describe the relative motion perpendicular to the orbital plane. The cross-track relative motion is described by a harmonic oscillation of amplitude $a\delta i$ and phase angle $u - \vartheta$.

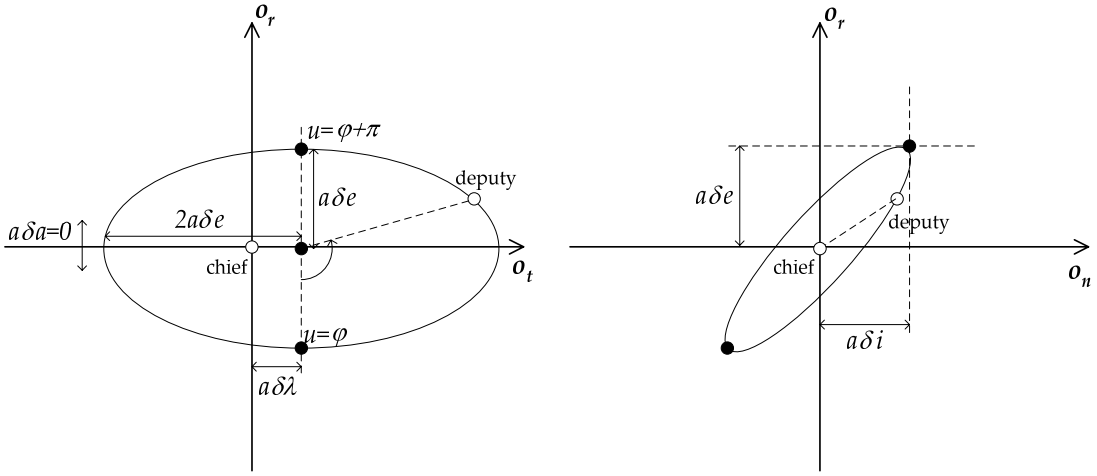


**Figure 1:** Projections of relative motion in the along-track/radial (left) and cross-track/radial (right) directions for arbitrary relative orbital elements with $\delta a = 0$.

The comparison between the general solution of the C-W equations in Eq. (4) and the first-order near-circular mapping between Hill coordinates and relative orbital elements in Eq. (5) demonstrates the equivalence between the C-W integration constants and the relative orbital elements. As shown in the next sections this correspondence paves the way to the design of straightforward guidance and control algorithms for formation-flying satellites in near-circular orbits. Apart from the gained geometrical insight, the interpretation of Eq. (4) in terms of relative orbital elements gives a useful tool to calculate the effects of impulsive velocity increments on the relative orbit. Furthermore the usage of relative orbital elements instead of position and velocity eases the incorporation of other relevant perturbations like Earth's oblateness and differential drag effects within the relative motion model as presented in the sequel.

## 1.2 Perturbed relative motion

The relative motion model described by Eq. (5) can be extended by considering $J_2$ perturbations of the orbital elements differences. The analytical treatment is based on the theory developed by Brouwer [12]. Here, only first-order terms in $J_2$ are retained, thus small errors of the order of $J_2^2$ and $e \cdot J_2$ are to be expected on top of the quadratic terms related to spacecraft separation and eccentricity discussed above. The secular variations of the relative orbital elements are easily obtained from the differentiation of the secular variations of the Keplerian orbital elements for each formation-flying satellite (i.e., chief and deputy spacecraft). The inclusion of these variations in Eq. (5) provides a relative motion model which constitutes a first order approximation of the solution of the equations of relative motion in the presence of $J_2$ perturbations. This is made possible by the fact that the short-period variations of the orbital elements are only a function of the mean argument of latitude and cancel out completely when computing the orbital elements differences for close (<10 km) formation flying satellites. In particular the first-order solution of the equations of relative motion for close formation-flying spacecraft in near-circular chief orbits in the presence of $J_2$ perturbations can be parameterized as

$$
\begin{aligned}
&\delta r_r / a = \delta a - \delta e \cos(u - \varphi - \varphi'(u - u_0)) \\
&\delta r_t / a = \delta \lambda - 10.5(\gamma \sin(2i)\delta i_x + \delta a / 7)(u - u_0) + 2\delta e \sin(u - \varphi - \varphi'(u - u_0)) \\
&\delta r_n / a = \delta i_x (\sin u - 3\gamma \sin^2 i (u - u_0)\cos u) - \delta i_y \cos u
\end{aligned}
\quad . \tag{6}
$$

The relative position is expressed as a function of the relative orbital elements at the initial time and the independent variable $u$. Due to the nature of the $J_2$ effects on the relative e/i-vectors, we have retained in Eq. (6) a polar notation for $\delta e$ but a Cartesian notation for $\delta i$. In fact the relative eccentricity vector evolves along a circle of radius $\delta e$ that is centered in the origin of the e-vector plane, with an angular velocity

$$
\varphi' = \frac{d\varphi}{du} = \frac{3J_2}{4(1-e^2)^2}\left(\frac{R_E}{a}\right)^2 (5\cos^2 i - 1) \quad . \tag{7}
$$

Here $R_E$ is the Earth's equatorial radius. The period of the relative e-vector motion is roughly 1000 times larger than the orbital period. For sun-synchronous formations with orbital inclinations of 97–102° and associated altitudes of 500–1500 km, Eq. (7) yields a clockwise motion of $\delta e$ with a period of roughly 100–200 days. The relative inclination vector is likewise affected by $J_2$ perturbations causing a secular shift of the orbital planes and thus a linear drift of $\delta i_y$. The secular motion of the relative e/i-vectors caused by the Earth oblateness is illustrated in Fig. 2. An initial configuration will ultimately be destroyed unless correction maneuvers are performed to compensate for the natural drift of both vectors.

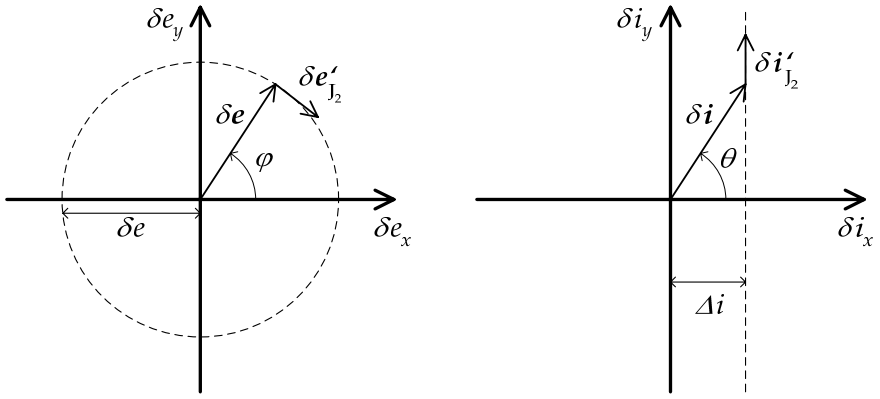


**Figure 2:** Secular evolution of the relative eccentricity (left) and inclination vectors (right).

The interaction of the upper atmosphere with the satellite's surface produces the dominant disturbance for LEO spacecraft after differential gravity. The relative along-track acceleration caused by drag for two formation-flying spacecraft is driven by the differences in their ballistic coefficients $\Delta B = (B_d - B)$, being $B = C_D A/m$, with $C_D$ the drag coefficient, $A$ the satellite cross-section area and $m$ the spacecraft mass. This causes an accumulated along-track offset which is a quadratic function of the elapsed time. In addition, the relative semi-major axis is linked to the derivative of the relative mean argument of latitude through the Kepler equation. This provides a drift of the radial separation which is proportional to the elapsed time. Overall the impact of differential drag on the relative motion can be expressed via the following terms which should be added to Eq. (6)

$$
\begin{aligned}
&\delta r_r = \Delta\dot{a}(t - t_0) \qquad = -\frac{2}{3n} a\Delta\ddot{u}(t - t_0) = -\frac{1}{n^2}\Delta B \rho v^2 (u - u_0) \\
&\delta r_t = \frac{1}{2} a\Delta\ddot{u}(t - t_0)^2 = \frac{3}{4n^2}\Delta B \rho v^2 (u - u_0)^2
\end{aligned}
\quad , \tag{8}
$$

where $\rho$ represents the upper atmosphere density and $v$ is the spacecraft velocity with respect to the atmosphere. According to Eq. (8), if the participating spacecraft are characterized by identical design with e.g. a differential ballistic coefficient below 2%, differential drag has evidently modest impact on the formation control during nominal operations in LEO orbits. On the other hand, this conclusion is no longer valid if one of the spacecraft enters a safe mode with uncontrolled yaw angle or the co-orbiting spacecraft are of different type and build. Depending on the specific geometry, the effective cross-section might increase and thus cause large differential drag accelerations of several hundred nm/s$^2$. When lasting over extended periods of time, a safe mode can thus cause notable change in along-track separation.

### 1.3 Relative orbit control

We consider an operational scenario with two formation-flying spacecraft in near-circular LEO. While the chief satellite is passive from a relative orbit control point of view, the deputy is performing orbit correction maneuvers. The proposed linearized relative motion model offers an ideal mathematical tool to process orbit maneuvers. In particular we can express the relative orbital elements as a function of the relative position and velocity by inverting the solution of the C-W equations given by Eq. (4). In particular, if we set $\delta r_\mathrm{r} = \delta r_\mathrm{t} = \delta r_\mathrm{n} = 0$ in Eq. (4), then the solution of the C-W equations describes the relative motion of a deputy spacecraft which is initially located at the same position of the chief spacecraft but with a different velocity. In other words the inversion of our linear relative motion model provides the direct relation between an instantaneous velocity increment in the Hill's orbital frame and the consequent change of the orbital elements as the following system of equations

$$\begin{aligned}
a\Delta\delta a &= +2\delta v_t / n \\
a\Delta\delta\lambda &= -2\delta v_r / n - 3(u - u_M)\delta v_t / n \\
a\Delta\delta e_x &= +\delta v_r \sin u_M / n + 2\delta v_t \cos u_M / n \\
a\Delta\delta e_y &= -\delta v_r \cos u_M / n + 2\delta v_t \sin u_M / n \\
a\Delta\delta i_x &= +\delta v_n \cos u_M / n \\
a\Delta\delta i_y &= +\delta v_n \sin u_M / n
\end{aligned} \quad , \tag{9}$$

commonly known as the Gauss' variational equations adapted to near-circular non-equatorial orbits [13]. Here the parameterization in terms of relative orbital elements introduced in the previous section has been adopted. The left hand terms correspond to the variations of the relative orbital elements induced by the instantaneous velocity changes $\delta v_\mathrm{r}$, $\delta v_\mathrm{t}$ and $\delta v_\mathrm{n}$, respectively in radial, along-track and cross-track directions (i.e., in the Hill's orbital frame). It is noted that the provided solution of the C-W equations describe the relationship between Cartesian relative coordinates at time $t$ and relative orbital elements at the initial time $t_0$, while the Gauss' variational equations provide the mapping between a velocity increment at time $t_0$ and the change of relative orbital elements at a later time $t$. Eq. (9) shows that for a given thrust, located at a specific mean argument of latitude $u_\mathrm{M}$, instantaneous variations of the actual relative orbital elements are generated, as well as a net change of mean longitude $a\Delta\delta\lambda$ within the time interval between the maneuver execution and the epoch of the relative orbital elements. As expected the control problem is fully decoupled with respect to in-plane and out-of-plane. Whereas a thrust in cross-track direction affects only the relative inclination vector, a thrust in the orbital plane (i.e., along-track and radial directions) influences the relative eccentricity vector, the relative semi-major axis and the relative longitude.

The goal of the relative orbit control system is to plan and execute correction maneuvers to ensure conformance with predefined nominal relative orbital elements $\delta\alpha^{\mathrm{nom}}$. The aim is to

maintain the actual orbital differences $\delta\boldsymbol{\alpha}$ confined within symmetric control windows centered on the nominal values $\left|\delta\alpha_i - \delta\alpha_i^{\text{nom}}\right| \le \delta\alpha_i^{\max}$, $i = 1,\ldots,6$.

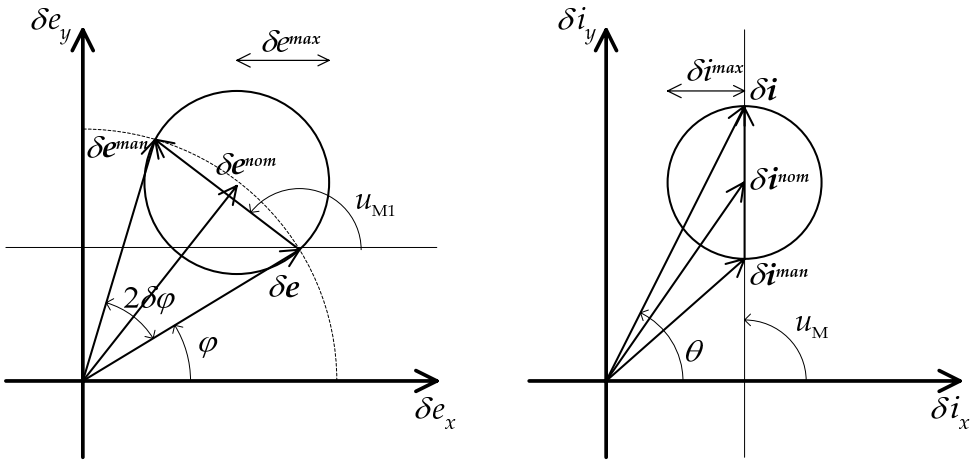


**Figure 3:** Graphical representation of in-plane (left) and out-of-plane (right) maneuver locations and relationship to the control windows for the relative eccentricity vector (left) and the relative inclination vector (right).

As explained in the previous section the relative eccentricity and inclination vectors are mainly affected by the Earth's oblateness perturbations. The former is characterized by a circular motion in the e-vector plane, the latter by a linear drift proportional to the inclination difference. We can take advantage of this natural secular motion and define convenient control windows for the relative e/i-vectors as depicted in Fig. 3. When the magnitudes of the relative e/i-vector tracking errors exceed the respective maximum allowed deviations, $\delta e^{\max}$ and $\delta i^{\max}$, the control scheme solves the Gauss' variational equations for the velocity increments and the location of the maneuvers along the orbit. The computed velocity increments will transfer the relative orbital elements to the opposite limit of the circular control window. Given the desired amplitude of the control windows and the absolute reference orbit in terms of eccentricity and inclination, the desired relative e/i-vectors after each orbit control maneuver can be determined uniquely. These are constants until a new nominal configuration or new control windows are prescribed. The guidance strategy ensures that the time between consecutive corrections of the relative e/i-vectors (i.e., the maneuver cycle) is maximized and represents as a consequence a fuel-efficient approach for formation maintenance. Depending on the desired control window, or equivalently on the required orbit control accuracy, along-track and cross-track maneuvers (in the form of single or double-pulses) are executed at regular time intervals in a deterministic fashion.

For the in-plane relative orbit control problem, minimum delta-v cost solutions of the Gauss' variational equations are provided by $u_{M1} - \xi = 0, \pi/2$ and $u_{M2} - u_{M1} = \pi$, being $\xi = \arctan(\Delta\delta e_y/\Delta\delta e_x)$. If $\Delta\delta a = \Delta\delta\lambda = 0$, the absolute minimum is given by $u_{M1} - \xi = 0$ and consists of pairs of along-track maneuvers separated by half an orbital revolution and executed in (anti-) flight direction. The size and location of the individual maneuvers can be expressed as follows

$$\begin{aligned}
\delta v_{t1} &= \frac{na}{4}\left[(\delta a^{\text{man}} - \delta a) + \left\|\delta \boldsymbol{e}^{\text{man}} - \delta \boldsymbol{e}\right\|\right] \\
\delta v_{t2} &= \frac{na}{4}\left[(\delta a^{\text{man}} - \delta a) - \left\|\delta \boldsymbol{e}^{\text{man}} - \delta \boldsymbol{e}\right\|\right] \\
u_{\text{M1}} &= \arctan[(\delta e_y^{\text{man}} - \delta e_y)/(\delta e_x^{\text{man}} - \delta e_x)]
\end{aligned} \quad . \tag{10}$$

Here the corrections of the relative eccentricity vector and semi-major axis have been expressed as the difference between their desired values after the two maneuvers, $\delta\boldsymbol{e}^{\text{man}}$ and

$\delta a^{\text{man}}$, and their actual values right before the execution of the first maneuver, $\delta e$ and $\delta a$ (cf. Fig. 3). The last two of Eq. (9) show that one cross-track maneuver is necessary and sufficient to control the out-of-plane relative motion and is given by

$$\begin{aligned} \delta v_n &= na\left\|\delta \boldsymbol{i}^{\text{man}} - \delta \boldsymbol{i}\right\| \\ u_{\text{M}} &= \arctan[(\delta i_y^{\text{man}} - \delta i_y)/(\delta i_x^{\text{man}} - \delta i_x)] \end{aligned}. \tag{11}$$

Note that once the nominal formation configuration and the size of the desired control window are fixed by design, the locations of the along-track and cross-track maneuvers are also known and constant during the mission. As shown in Fig. 3 the first along-track maneuver and the cross-track maneuver are located at a mean argument of latitude that matches the phase of the relative e/i-vector corrections. This characteristic of the control law is of extreme relevance when designing a formation of spacecraft with the aim of minimum complexity and operational effort.

The formation maintenance strategy described here can be used as well for formation reconfiguration. One has to prescribe the desired nominal relative orbital elements and compute size and locations of the necessary orbit control maneuvers in along-track and cross-track direction respectively. The drawback of this control scheme is given by the undesired variation of the mean argument of latitude that is always induced by the first tangential pulse. In the case of large formation reconfigurations or acquisitions this effect can become unacceptably large. An alternative approach for formation reconfiguration can achieve a more accurate formation reconfiguration, avoiding large drifts of the mean along-track separation, by the use of maneuvers in radial direction. Although the radial pulses are two times less fuel-efficient than the tangential maneuvers (cf. Eq. (9)), they do not produce any variation of the semi-major axis, and as a consequence are inherently more accurate with respect to along-track control.

The alternative control scheme is based on the choice of $u_{\text{M1}} - \xi = \pi/2$. In this case the double impulse solution of Eq. (9) represents a local minimum and reduces to

$$\begin{aligned} \delta v_{r1} &= \frac{na}{2}\left[-(\delta\lambda^{\text{man}} - \delta\lambda)/2 + \left\|\delta \boldsymbol{e}^{\text{man}} - \delta \boldsymbol{e}\right\|\right] \\ \delta v_{r2} &= \frac{na}{2}\left[-(\delta\lambda^{\text{man}} - \delta\lambda)/2 - \left\|\delta \boldsymbol{e}^{\text{man}} - \delta \boldsymbol{e}\right\|\right] \\ u_{\text{M1}} &= \arctan[(\delta e_x^{\text{man}} - \delta e_x)/(\delta e_y^{\text{man}} - \delta e_y)] \end{aligned}. \tag{12}$$

Obviously the presented reconfiguration algorithm can not compensate for the drift of the relative semi-major axis caused by differential drag. Radial maneuvers cannot correct the semi-major axis, thus a net difference between chief and deputy semi-major axis will accumulate over time and induce a gradually increasing variation rate of the mean along-track separation. This side effect has to be taken into account only if the presented control scheme is applied to achieve more accurate, but more expensive, formation maintenance. In this case we can simply introduce aside Eq. (12), at the same maneuver locations, small tangential maneuvers to compensate for semi-major axis changes only.

## 2 GPS-BASED RELATIVE NAVIGATION

Section 1 presented a safe and fuel-efficient guidance and control strategy for formation flying spacecraft. The treatment assumes an ideal knowledge of the absolute and relative orbit available on-board in the computation of the analytical closed-form feedback control law. The assumption of ideal navigation sensors is abandoned in this chapter which is devoted to the

problem of real-time GPS-based absolute and relative positioning of co-orbiting satellites. We address the design of an on-board navigation system aiming at the provision of absolute and relative position and velocity for the PRISMA space-segment which consists of two satellites (namely *Main* and *Target*) flying in formation in LEO. The navigation software has to be integrated and executed on a spacecraft on-board computer with limited memory and computational capacity. The available GPS receivers offer raw measurements of C/A-code pseudorange and L1 integrated carrier phase which have to be processed as soon as they are received in a reduced-dynamic sequential estimation algorithm. The absolute and relative orbit determination and prediction accuracy requirements drive the selection of the applied force model and measurement concept. Furthermore, the widely varying formation flying scenarios necessitate a high level of robustness and flexibility of the navigation system which shall handle thruster pulses of the propulsion system and operate properly in the presence of GPS data gaps caused for example by power constraints or spacecraft reorientation phases.

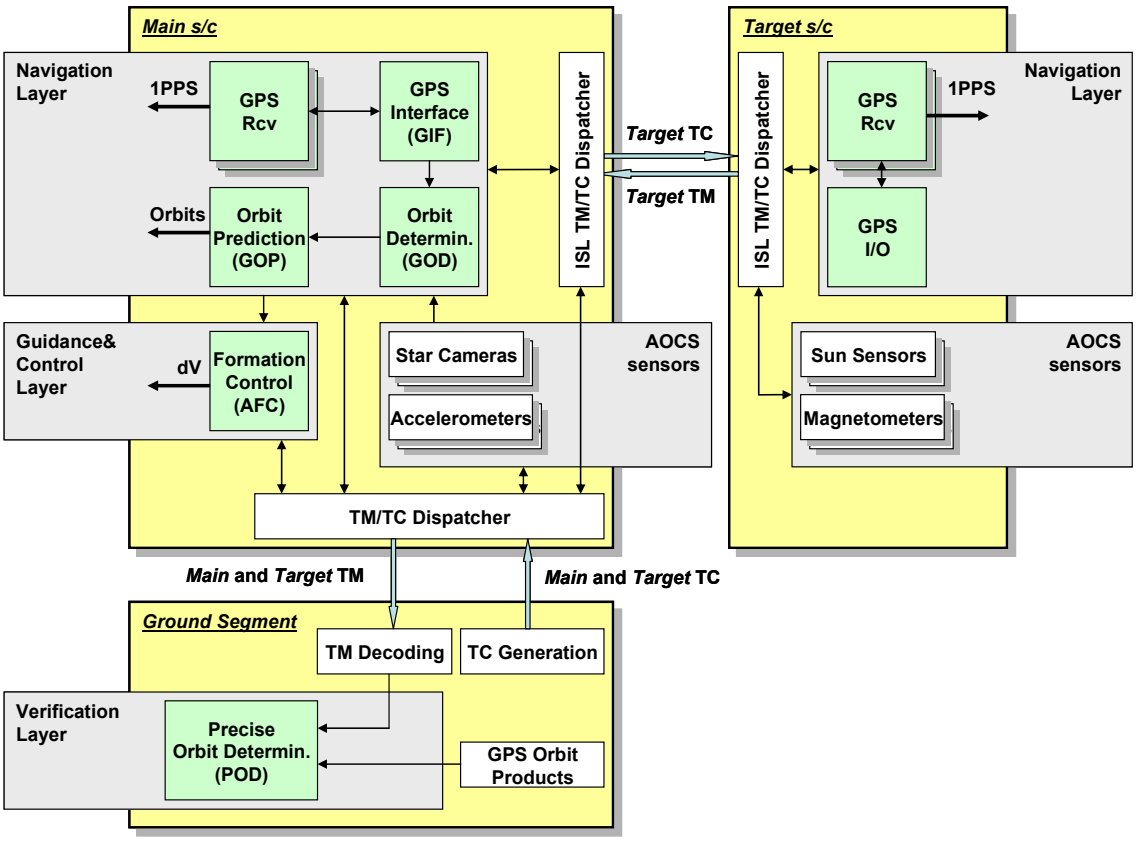


**Figure 4:** Top-level functional view of the GPS-based guidance, navigation and control system developed for PRISMA. The *Main* and *Target* spacecraft as well as the ground-segment are enclosed in yellow rectangles. Hardware and software elements strictly related to GPS are green. Interfaces to other subsystems of the space-segment are gray. The provided architecture is simplified and focuses on GPS related functions. On-board signal conditioning and filtering related to AOCS sensors measurements are not shown.

## 2.1 Top-level functional view

A top-level functional view of the GPS-based guidance, navigation and control system developed for PRISMA is presented in Fig. 4. The DLR's GPS receivers will provide raw single-frequency data to the navigation subsystem and deliver a Pulse Per Second for the synchronization of the on-board clock. The use of GPS data from both spacecraft implies an inter-satellite link between *Main* and *Target*. The navigation filter is implemented on *Main* and provide the desired absolute and relative orbit information in real-time to the various PRISMA experiment users. Among them, Fig. 4 shows the Autonomous Formation Control experiment (AFC) which makes use of the algorithms defined in the previous chapter to compute output control requests to the *Main* propulsion system. The GPS-based navigation

system is naturally split into three modules devoted to the input/output interfacing of the GPS receivers (GIF), to the GPS-based Orbit Determination (GOD) and to the GPS-based Orbit Prediction (GOP). Additional interfaces with attitude sensors and accelerometers are foreseen to handle the offsets of the GPS antennas with respect to the spacecraft center of mass and the orbit control maneuvers, respectively. GPS data as well as auxiliary attitude and maneuver info will be downloaded during ground-station contacts and provided to the Precise Orbit Determination (POD) function which is used for the on-ground post-facto highly precise reconstruction of the formation absolute and relative orbits. The POD products will be required for the a posteriori evaluation of sensor data and the validation of the formation flying experiments.

### 2.2 Estimation concept

The concept that has been shown to better satisfy the requirements and goals for the PRISMA mission is a combined Extended Kalman Filter (EKF) processing of GRAPHIC (GR) and single difference carrier phase (SDCP) data types. Compared to the other alternatives this concept suffers from a relatively high computational load and complexity, but guarantees good navigation accuracy, robustness to attitude uncertainty and different GPS antenna orientations, simplicity in filter initialization and maneuver handling. The selected filter estimation parameters

$$\boldsymbol{y} = \left( (\boldsymbol{x}; \boldsymbol{p}; c\delta t; \boldsymbol{N})^{\mathrm{M}}; (\boldsymbol{x}; \boldsymbol{p}; c\delta t; \boldsymbol{N})^{\mathrm{T}}; \delta \boldsymbol{v} \right) \tag{13}$$

comprise the 6-dimensional spacecraft state in the ECI frame $\boldsymbol{x}$, the scalar GPS receiver clock offset $c\delta t$, a fixed number of force model parameters $\boldsymbol{p}=(C_{\mathrm{D}};\boldsymbol{a}_{\mathrm{emp}})$, including the aerodynamic drag coefficient $C_{\mathrm{D}}$ and 3 empirical accelerations $\boldsymbol{a}_{\mathrm{emp}}$ in the local orbital frame, and the 12 GRAPHIC float biases $\boldsymbol{N}$ for each GPS receiver channel. Next to these 23 parameters, which are estimated for each of the co-orbiting spacecraft (superscripts M and T for the *Main* and *Target* spacecraft, respectively), we decide to include the 3 *Main* orbit maneuver increments $\delta\boldsymbol{v}$ expressed again in the local orbital frame for a total filter size of $n$ = 49. This approach gives the possibility to incorporate the orbit control maneuvers within the navigation process through their direct estimation, and to take into account deficiencies of the maneuver model via dedicated white or colored process noise. Note that we have decided to remove the vertical ionospheric path delay from the estimation state vector. In fact the adopted GPS data types can be considered as ionosphere-free combinations for small inter-satellite separations (<5 km) [8]. The selected GPS measurements vector

$$\boldsymbol{z} = \left( \rho_{GR}^{M}; \rho_{GR}^{T}; \rho_{SDCP} \right) \tag{14}$$

comprises a maximum of 12 GRAPHIC data types taken by the *Main* spacecraft receiver, a maximum of 12 GRAPHIC data types taken by the *Target* spacecraft receiver, and a maximum of 12 single difference carrier phase measurements related to the GPS satellites which are commonly visible by the two spacecraft. The maximum number of processed observations is given by $m$ = 36 and provides a high level of redundancy to the filter because GRAPHIC and SDCP observations which involve the same GPS satellites are not independent.

## 3 FORMATION FLYING TESTBED

### 3.1 System testing and validation

The PRISMA integrated system testing is based on the SATellite LABoratory (SATLAB) facility at the Swedish Space Corporation (SSC) [14]. SATLAB is a software/hardware

laboratory providing a unified configurable simulation environment for use in several applications within the PRISMA project. The supported system level simulations can typically consist of 1) Software system tests to verify the required functionality of the on-board software. 2) Closed-loop tests involving the integrated Flight Model (FM) spacecraft. 3) Closed-loop tests involving different levels of Engineering Model (EM) or FM hardware-in-the-loop. 4) Test development on a system level simulator. 5) Development of operational procedures in a system level simulator. 6) Operator training by means of system level simulations. 7) Test results and flight results analysis.

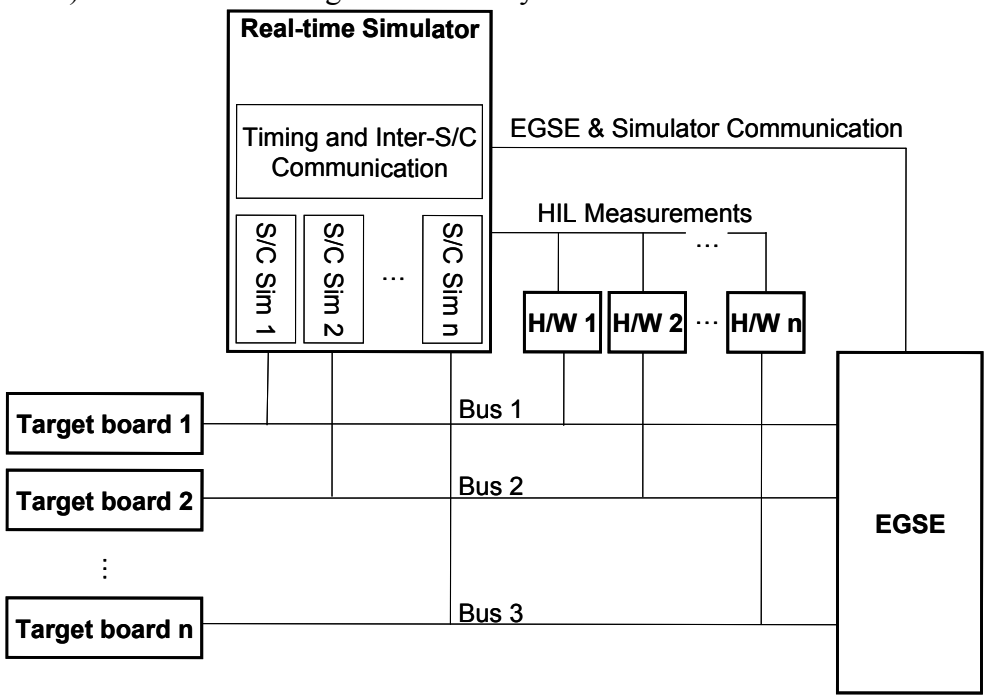


**Figure 5:** General SATLAB configuration at SSC.

The simulation environment runs the OBS on flight representative target hardware (i.e., EM or FM on-board computers), and includes different levels of hardware-in-the-loop (HIL). SATLAB supports simultaneous simulations of several spacecraft in formation flying. Fig. 5 illustrates the most general configuration of SATLAB. The figure shows how several spacecraft can be simulated, each with its own target computer and communication bus. The figure also shows how hardware is included in the loop for each of the simulated spacecraft and how these can be commanded or read from the simulator. The communication link between the Electrical Ground Support Equipment (EGSE) and the simulator is also indicated in the figure. The real-time environment implemented in SATLAB resides in the simulator and the target computers. In particular the simulator is a standard desktop PC, treated as a Matlab/Simulink xPC target, while the target platforms are LEON3 FT processors. The backbone of the software system is the Real Time Workshop (RTW) Embedded Coder by which the real time applications are auto-coded and launched on the target units.

## 3.2 Formation Control Experiment Rehearsal

Within the GPS-based GNC system development discussed in this research, a series of real-time HIL tests have been conducted at various stages to verify the proper integration of the flight software within the on-board software and computer. Through these tests, it has been possible to verify communication, telemetry and telecommand, interface and functionalities of the integrated flight software. Results from a representative HIL test conducted in the SATLAB facility (March 17 to March 24, 2008) are presented in the sequel. The scope of the test is to verify the performance of the GPS-based GNC software integrated in the PRISMA on-board computer. The test strategy tries to stimulate the software modules in order to enable

the execution of most of the available functionalities and execution paths. For this campaign, the SATLAB facility setup includes EM on-board computers, the complete on-board software and the Telemetry/Telecommand (TM/TC) network. The GPS receivers are modeled through a realistic software emulator integrated in the real-time simulator (cf. Fig. 5).
The AFC closed-loop activities foresee four formation flying configurations. Each constellation covers a time arc of 24 hours. AFC has to autonomously acquire and maintain the desired configurations for the prescribed period of time. Table 1 lists the desired formation geometries in terms of relative orbital elements as provided to AFC via TC. The commanded control windows for the relative eccentricity and inclination vectors are kept constant during the complete test and are given by $a\delta e^{\max} = a\delta i^{\max} = 2$m. The initial relative geometry corresponds to non-parallel relative eccentricity/inclination vectors with relative perigee and relative ascending node at 100° and 40° respectively. These angles are modified in the second formation flying configuration which is characterized by a relative eccentricity vector aligned with the y-axis and a relative inclination vector at 60° phase. Parallel relative eccentricity/inclination vectors are applied in the third and fourth configurations which differ by a mean along-track separation of 300 m.

**Table 1:** Four formation flying configurations to be maintained and acquired autonomously by AFC.

| | Nominal relative orbital elements and phase angles | | | | | | | |
|---|---|---|---|---|---|---|---|---|
| Time frame | $a\delta a^{\text{nom}}$ [m] | $a\delta\lambda^{\text{nom}}$ [m] | $a\delta e_x^{\text{nom}}$ [m] | $a\delta e_y^{\text{nom}}$ [m] | $\varphi^{\text{nom}}$ [°] | $a\delta i_x^{\text{nom}}$ [m] | $a\delta i_y^{\text{nom}}$ [m] | $\vartheta^{\text{nom}}$ [°] |
| Config. 1 | 0 | 0 | -34.7296 | 196.9616 | 100 | 76.6044 | 64.2788 | 40 |
| Config. 2 | 0 | 0 | 0 | 200 | 90 | 50 | 86.6025 | 60 |
| Config. 3 | 0 | 0 | 0 | 300 | 90 | 0 | 100 | 90 |
| Config. 4 | 0 | 300 | 0 | 300 | 90 | 0 | 100 | 90 |

The accuracy of the real-time navigation filter during the 4-day formation control rehearsal is evaluated by subtracting the position and velocity of the *Main* and *Target* spacecraft provided by GOP from the true reference trajectory logged from the SATLAB real-time simulator in the ECEF reference frame at 10 s samples. The relative navigation errors are then mapped in the orbital frame and plotted in Fig. 6. Upon filter convergence, and excluding the formation reconfiguration phases, the obtained absolute and relative navigation accuracy for the position is 3.2 m and 7.8 cm (3D, RMS) respectively. The relative orbit control errors, or control tracking error, are computed by subtracting the actual relative motion of *Main* with respect to *Target* from the desired relative motion as described by the selected nominal relative orbital elements (cf. Table 1). As shown in Fig. 7, during formation keeping phases, the relative position control errors stay below 5.0/25.0/2.5 m in radial, along-track and cross-track directions respectively. A net improvement of the control performance can be observed when switching from the first to the next formation flying configurations. This effect is especially visible in along-track direction and is due to the activation of the radial closed-loop mode which implements maneuvers in radial direction (cf. Eq. (12)). This avoids offsets of the relative semi-major axis and unintentional drifts of the relative mean argument of latitude at a higher fuel consumption cost.
Overall a total of 43 pairs of in-plane maneuvers and 17 out-of-plane maneuvers are issued by AFC to maintain the formation geometry and reconfigure it when required from ground. The delta-v size is typically at the millimeter level for formation maintenance and at the centimeter level for formation reconfiguration as foreseen by the adopted analytical model. As expected the number of out-of-plane formation keeping maneuvers is reduced to zero for configurations with $\Delta i = 0$ (i.e., identical spacecraft inclination).

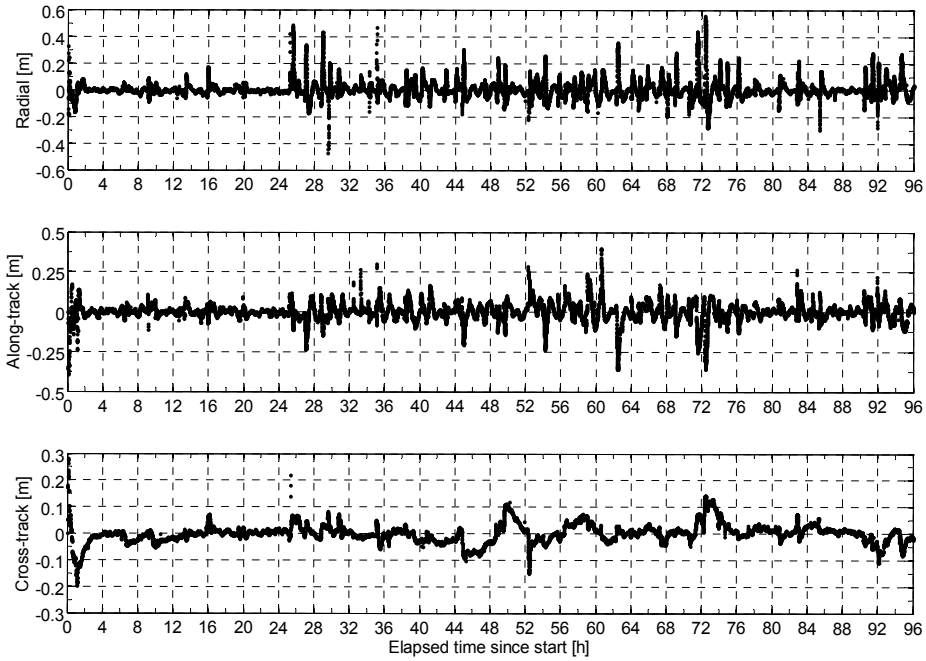


**Figure 6:** Relative position error (i.e., *Main* with respect to *Target*) mapped into the orbital frame aligned with the radial (top), along-track (middle) and cross-track (bottom) directions.

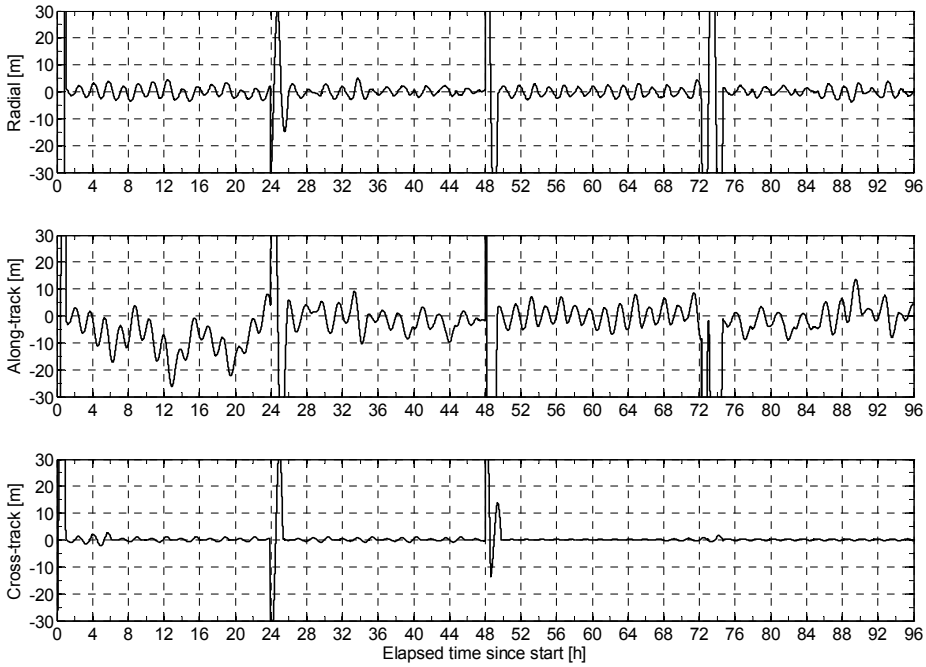


**Figure 7:** Control tracking error mapped into the orbital frame aligned with the radial (top), along-track (middle) and cross-track (bottom) directions.

## 4 CONCLUSION

The main goal of this research was to design, implement and test an innovative GPS-based guidance, navigation and control system for two-satellite formations in low Earth orbit. The results from the previous section give a clear demonstration that this objective has been fulfilled. In particular the direct outcome of the work presented here is a flight-ready spaceborne autonomous formation flying system which has been integrated into the Swedish PRISMA technology demonstration mission.

The resulting contributions to the body of knowledge are manifolds and, as re-proposed in the sequel, influence mainly the areas of impulsive relative orbit control and combined GPS-

based absolute/relative navigation. Section 1 has investigated a formation-flying concept able to realize the demanding baselines for aperture synthesis, while minimizing the collision hazard associated with proximity operations. The parameterization in terms of relative orbital elements, originally developed for geostationary satellites, has been successfully extended to LEO formations. It provides immediate insight into key aspects of the relative motion and is particularly useful for orbit control purposes and proximity analysis. Section 2 has presented the GPS-based navigation system in terms of filter structure, adopted measurements and state parameters. The unified filter design has several advantages over classical navigation concepts available in literature. The full information content provided by the available measurements can be exploited to its largest extent. In fact no strict requirement on common GPS satellite visibility is necessary to provide relative state estimates. Furthermore, initialization and maneuver handling is much simplified if compared to split filters dedicated to the independent reconstruction of absolute and relative states.

A sophisticated formation flying testbed has been used to perform realistic integrated closed-loop tests at system level. The relative navigation accuracy depends critically on the attitude profile during specific mission phases and may range from a worst case accuracy of around 0.5 m if the GPS antennas of *Main* and *Target* point in different directions down to a few cm if a sufficient number of common GPS satellites is tracked by the two spacecraft. A realistic assessment of the control tracking errors shows full compliance to the requirements with maximum errors during formation keeping phases of 5.0/25.0/2.5 m in radial, along-track and cross-track directions respectively. Overall the obtainable control accuracy is driven by the impulsive feedback algorithm itself, which relies on pairs of maneuvers separated by half an orbital revolution, rather than sensor and actuator errors. Anyhow the resulting control system can be considered as an optimal choice in view of the prescribed objectives. In fact, it provides the desired control accuracy through a minimum number of thrust activations, a reduced propellant consumption, minimum collision risk, utmost simplicity and predictability.

## REFERENCES


[1] Hill G. W.; “Researches in the Lunar Theory”, American Journal of Mathematics, Vol. 1, pp. 5-26, 1878.

[2] Kasdin N. J., Kolemen, E.; “Bounded, Periodic Relative Motion Using Canonical Epicyclic Orbital Elements”, American Astronautical Society, Paper 05-186, Jan. 2005.

[3] Eckstein M. C., Rajasingh C.K., Blumer P.; “Colocation Strategy and Collision Avoidance for the Geostationary Satellites at 19 Degrees West”, International Symposium on Space Flight Dynamics; 6-10 Nov. 1989, CNES, Toulouse 1989.

[4] D’Amico S., Montenbruck O.; “Proximity Operations of Formation-Flying Spacecraft Using an Eccentricity/Inclination Vector Separation”, Journal of Guidance, Control, and Dynamics, Vol. 29, No. 3, May-June 2006.

[5] Montenbruck O., Kirschner M., D’Amico S., and Bettadpur S.; “E/i-vector separation for safe switching of the GRACE formation”, Aerospace Science and Technology, 10(7):628–635, 2006.

[6] Leung S.; “High Precision Real-Time Navigation for Spacecraft Formation Flying Using Spaceborne GPS Technology”, PhD thesis, School of Aerospace, Mechanical and Manufacturing, Technology, Faculty of Engineering, RMIT University, 2003.

[7] Yunck T. P.; “Coping with the atmosphere and ionosphere in precise satellite and ground positioning”, Environmental Effects on Spacecraft Positioning and Trajectories, 73, 1993.

[8] van Barneveld P.W.L., Montenbruck O., and Visser P.N.A.M; “Differential ionospheric effects in GPS based navigation of formation flying spacecraft”, 3rd International Symposium on Formation Flying, Missions and Technologies, Noordwijk, The Netherlands, April 2008.

[9] Persson S., Bodin P., Gill E., Harr J., and Jörgensen J.; “PRISMA–an autonomous formation flying mission”, ESA Small Satellite Systems and Services Symposium (4S), Sardinia, Italy, September 2006.

[10] Clohessy W., Wiltshire R.; “Terminal Guidance Systems for Satellite Rendezvous”, Journal of Aerospace Sciences, Vol. 27, pp. 653-658, 1960.

[11] Schaub H.; “Relative orbit geometry through classical orbit element differences”, Journal of Guidance, Control and Dynamics, 27(5), September–October 2004.

[12] Brouwer D.; “Solution of the problem of artificial satellite theory without drag. Astronomical Journal, 64(1274):378–397, 1959.

[13] Micheau P.; “Orbit Control Techniques for Low Earth Orbiting (LEO) Satellites”, Chap. 13 in Carrou J.P. ed, Spaceflight Dynamics, Cepadues-Editions, Toulouse, France, 1995.

[14] Bodin P.; “SATLAB Specification”, Technical Report SPC31500-S25, Version 1.0, Swedish Space Corporation, Solna, 2005.



◄ BACK TO SESSION DETAILED CONTENTS ◄ BACK TO HIGHER LEVEL CONTENTS